SMC-TR-02-09

AEROSPACE REPORT NO.
TR-2001(1306)-4

Combustion of Nitrogen in Low-Pressure H_2+O_2 and H_2+CO+O_2 Flames

30 November 2001

Prepared by

P. M. SHEAFFER and P. F. ZITTEL
Space Science Applications Laboratory
Laboratory Operations

Prepared for

SPACE AND MISSILE SYSTEMS CENTER
AIR FORCE SPACE COMMAND
2430 E. El Segundo Boulevard
Los Angeles Air Force Base, CA 90245

Systems Planning and Engineering Group

APPROVED FOR PUBLIC RELEASE;
DISTRIBUTION UNLIMITED

THE AEROSPACE CORPORATION
EL SEGUNDO, CALIFORNIA

This report was submitted by The Aerospace Corporation El Segundo CA 90245-4691 under Contract No. F04701-00-C-0009 with the Space and Missile Systems Center, 2430 E. El Segundo Blvd., Los Angeles Air Force Base, CA 90245. It was reviewed and approved for The Aerospace Corporation by Dr. H. F. Bittner, Principal Director, Systems Acquisitions Support, Office of Chief Architect/Engineer, Systems Planning and Engineering Group. Mr. Dan Pilson, SMC/AXFV, was the project officer for the program.

This report has been reviewed by the Public Affairs Office (PAS) and is releasable to the National Technical Information Service (NTIS). At NTIS, it will be available to the general public, including foreign nationals.

This technical report has been reviewed and is approved for publication. Publication of this report does not constitute Air Force approval of the report's findings or conclusions. It is published only for the exchange and stimulation of ideas.

Dan Pilson
SMC/AXFV

REPORT DOCUMENTATION PAGE

Form Approved
OMB No. 0704-0188

Public reporting burden for this collection of information is estimated to average 1 hour per response, including the time for reviewing instructions, searching existing data sources, gathering and maintaining the data needed, and completing and reviewing this collection of information. Send comments regarding this burden estimate or any other aspect of this collection of information, including suggestions for reducing this burden to Department of Defense, Washington Headquarters Services, Directorate for Information Operations and Reports (0704-0188), 1215 Jefferson Davis Highway, Suite 1204, Arlington, VA 22202-4302. Respondents should be aware that notwithstanding any other provision of law, no person shall be subject to any penalty for failing to comply with a collection of information if it does not display a currently valid OMB control number. **PLEASE DO NOT RETURN YOUR FORM TO THE ABOVE ADDRESS.**

1. REPORT DATE (*DD-MM-YYYY*)
30-11-2001

2. REPORT TYPE

3. DATES COVERED *(From - To)*

4. TITLE AND SUBTITLE

Combustion of Nitrogen in Low-Pressure H_2+O_2 and H_2+CO+O_2 Flames

5a. CONTRACT NUMBER
F04701-00-C-0009

5b. GRANT NUMBER

5c. PROGRAM ELEMENT NUMBER

6. AUTHOR(S)

P. M. Sheaffer and P. F. Zittel

5d. PROJECT NUMBER

5e. TASK NUMBER

5f. WORK UNIT NUMBER

7. PERFORMING ORGANIZATION NAME(S) AND ADDRESS(ES)

The Aerospace Corporation
Laboratory Operations
El Segundo, CA 90245-4691

8. PERFORMING ORGANIZATION REPORT NUMBER

TR-2001(1306)-4

9. SPONSORING / MONITORING AGENCY NAME(S) AND ADDRESS(ES)
Space and Missile Systems Center
Air Force Space Command
2430 E. El Segundo Blvd.
Los Angeles Air Force Base, CA 90245

10. SPONSOR/MONITOR'S ACRONYM(S)
SMC

11. SPONSOR/MONITOR'S REPORT NUMBER(S)
SMC-TR-02-09

12. DISTRIBUTION/AVAILABILITY STATEMENT
Approved for public release; distribution unlimited.

13. SUPPLEMENTARY NOTES

14. ABSTRACT

Among other tools, the Air Force employs computer models of the chemistry in afterburning rocket plumes to assess the environmental impact of rocket launches on the upper atmosphere and, in particular, the ozone layer. To improve the accuracy of these models, it is necessary to verify the chemical mechanisms and reaction rate constants used in the models. One method by which verification can be achieved is by comparing the results of laboratory flame measurements with model predictions of combustion products.

Nitrogen is present in the atmosphere at all altitudes and is entrained with oxygen into the afterburning exhaust plume of a rocket motor as it rises through the troposphere and lower stratosphere. In the laboratory, we have examined the low-pressure combustion of nitrogen-doped H_2 + O_2 and H_2 + CO + O_2 flames. The experiments were carried out at a pressure of 50 Torr, simulating rocket plume afterburning conditions at 20 km altitude. The cool, post-flame combustion products were analyzed with a mass spectrometer and a specially modified NO_x chemiluminescence analyzer, as the stoichiometry of the flame was varied to simulate the range of afterburning mixtures encountered in a real rocket plume. Comparisons of the experimental results with preliminary computer flame simulations are used to test the accuracy of the chemical mechanisms employed in modeling nitrogen combustion at low pressures.

15. SUBJECT TERMS
Rocket plume, Afterburning, Environmental impact, Nitrogen oxides, Combustion

16. SECURITY CLASSIFICATION OF:			17. LIMITATION OF ABSTRACT	18. NUMBER OF PAGES	19a. NAME OF RESPONSIBLE PERSON
					Patti Sheaffer
a. REPORT	b. ABSTRACT	c. THIS PAGE			19b. TELEPHONE NUMBER *(include area code)*
UNCLASSIFIED	UNCLASSIFIED	UNCLASSIFIED		23	(310)336-7349

Standard Form 298 (Rev. 8-98)
Prescribed by ANSI Std. 239.18

Acknowledgments

The authors express their gratitude to Dr. G. Ternet of The Aerospace Corporation for suggesting the NO_x chemiluminescence detection technique and Dr. K. Westburg of The Aerospace Corporation for advice and valuable discussions on adapting his analyzer for use in our experiment, interpreting the data, and assisting in the calibration of the analyzer.

Contents

1. Introduction 1
2. Flame Experiments 3
   - 2.1 Description 3
   - 2.2 Results 6
3. Flame Model 9
   - 3.1 Description 9
   - 3.2 Model Results 9
4. Discussion 11
5. Summary 13

References 15

Appendix 17

Figures

1. Photograph of the low-pressure flame chamber 3
2. Diagram of the low-pressure flame apparatus 4
3. Argon signal vs radial position of sample tube 5
4. NO and NO_x yields as a function of flame stoichiometry for H_2-fueled flame 7
5. NO and NO_x yields as a function of flame stoichiometry for H_2+CO fueled flame 8
6. Modeled NO and NO_x yields for H_2-fueled flame. 10
7. Modeled NO and NO_x yields for a 1:1 H_2+CO fueled flame. 10

Table

1. Model Input Flows (SLM) 9

1. Introduction

The Air Force's commitment to protecting the environment has generated significant interest in the potential environmental impact of its launch vehicle fleet, an important aspect of which is the effect of rocket plume exhaust on the Earth's stratospheric ozone layer. The Air Force increasingly relies on computer model simulations of the chemistry in afterburning rocket plumes to accurately predict environmental impacts. This requires that the chemical mechanisms and reaction rate constants used in the rocket plume models be verified at stratospheric pressures before the model predictions can be trusted. Verification can be carried out by using proposed chemical mechanisms in model simulations of laboratory flame experiments and then comparing the model predictions with the experimental results. The validated mechanisms and rates can then be used in detailed models of afterburning in supersonic rocket plumes.

In the past, we have investigated aspects of chlorine,[1] sulfur,[2,3] and nitrogen[4] chemistry under simulated plume afterburning conditions with computer models and laboratory experiments. In this report, we describe new measurements of the combustion of nitrogen in a plume afterburning environment to produce oxides of nitrogen. The experimental measurements and companion model calculations are initial efforts and will be refined as the study progresses.

The primary combustible species present in the exhaust of rocket motors are hydrogen (H_2) and carbon monoxide (CO). H_2 is abundant in nearly all liquid- and solid-fueled rocket exhausts since nearly all propellant combinations contain hydrogen atoms and are formulated to burn somewhat fuel rich. CO is a significant exhaust product when the propellant mixture contains carbon, which is true for nearly all liquid and solid propellant combinations with the obvious exception of LOX/ H_2. Afterburning occurs when the surrounding atmosphere is entrained into the hot plume downstream of the rocket, and the combustibles are oxidized to H_2O and CO_2. Thus, the study of pollutant production through afterburning is essentially a study of the chemistry of the pollutant species in the environment of an H_2+O_2, or H_2+CO+O_2, flame at pressures and compositions characteristic of the rocket plume environment. The results of such studies are applicable to essentially all propellant types.

Nitrogen oxide species can be generated within the rocket motor itself when nitrogen is present in the propellant mixture and also by afterburning as ambient nitrogen and oxygen are incorporated into the downstream plume. NO_x species deposited in the wake of the plume can participate in catalytic cycles to convert ozone to O_2. NO reacts rapidly with ozone in the stratosphere. NO_2 is easily photodissociated to form NO and can also combine with ClO to form $ClONO_2$, a night-time reservoir for Cl atoms that can be liberated in the ensuing day by photolysis. $ClONO_2$ is also a potential precursor to HNO_3. Adsorbed nitrogen acids may chemically activate (or poison) particulate surfaces. It is, therefore, important to have accurate chemical models to calculate the production of NO, NO_2, and other NO_x species by rocket plume afterburning reactions at stratospheric pressures.

Combustion has been studied with modern scientific methods for over 100 years, yet remains difficult to model due to the stiff (exponential) nature of the chemical kinetic equations governing the chemistry and the complicated fluid dynamics of real flames.[5,6] Combustion phenomena are generally divided into two temperature regimes, hot and cool combustion, between which lies a transition region that varies in extent depending on the chemical system of the flame. Hot combustion is typically associated with visible flames, and this region may heat up to several thousands of degrees Kelvin. In cool combustion, reactions usually proceed relatively slowly with only minor changes in temperature and pressure, and a visible flame may or may not be observed. Depending on the chemical system, this region may extend down to temperatures of a few hundred degrees Kelvin. From the standpoint of pollutant production, the relevant region of afterburning in real rocket plumes covers the full range of temperatures from hot to cool combustion. This makes afterburning complicated to model since chemical reaction rates may not be known accurately for all important reactions over the entire temperature range. Our laboratory flame experiments are configured to examine the ultimate products of both hot and cool combustion by measuring the cooled, downstream post-reaction products of the flame. Although the hottest, radical-rich part of the flame is not directly sampled, the stable post-flame products reflect all of the flame chemistry and are directly relevant to the residues deposited in cool rocket plume wakes.

The experimental flame measurements are intended to be compared with the predictions of flame model calculations to test the accuracy of the chemical mechanisms and reaction rate constants that impact pollutant production. In this study, preliminary flame simulations were run with the one-dimensional CHEMKIN/PREMIX flame model, although more complex computational fluid dynamic models of the laboratory flame are planned for the future. The fundamental mechanisms and reaction rate constants validated by these procedures can then be employed in any flame model. In particular, the results are transferable to computer codes formulated to simulate mixing and afterburning in full-scale, supersonic rocket plumes.

2. Flame Experiments

2.1 Description

The low-pressure flame apparatus is pictured in Figure 1. The flame chamber is fabricated from stainless steel with several access ports and windows for sampling flame species and radiant emission. In the figure, the face of the burner may be seen through the viewport, and the quartz microprobe sampling tube is seen in the upper left-hand corner. Figure 2 illustrates the interior of the flame chamber. A flame is stabilized at the top face of a McKenna sintered bronze burner. Fuel and oxygen are mixed within the burner before combustion, forming the core gas flow that exits the burner in a circular region of 6.1 cm diameter. In the context of these experiments, "fuel" refers to either H_2, or an H_2+CO mixture, which are the fuels for the laboratory flame, as well as a typical afterburning rocket plume. The reactant flows are metered with electronic mass flow meters/controllers to maintain constant flame stoichiometry while measurements are made. The core flame is surrounded by a flowing argon gas shroud in a ring around the burner core and by a quartz sleeve to confine the flame so that it approximates one-dimensional flow for some distance downstream. The quartz liner

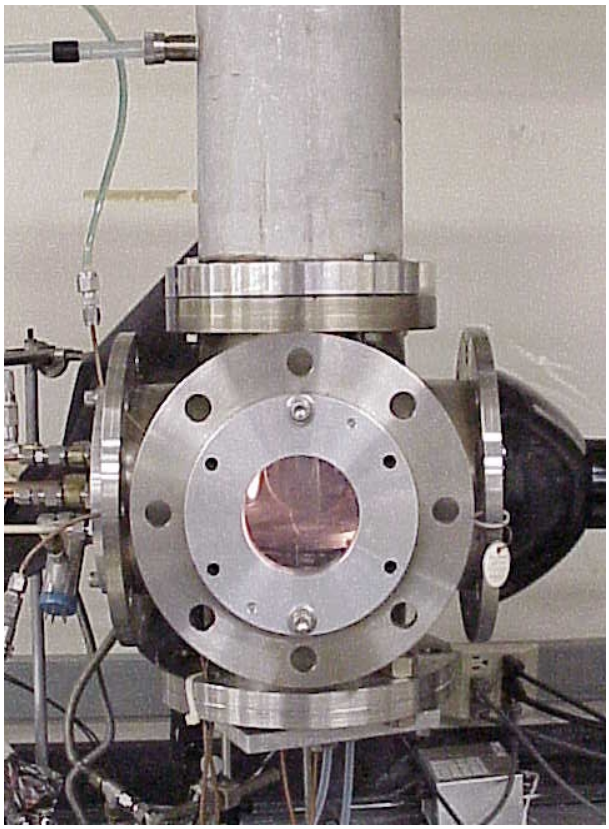

Figure 1. Photograph of the low-pressure flame chamber. The quartz microprobe sampling tube can be seen in the upper left of the photograph.

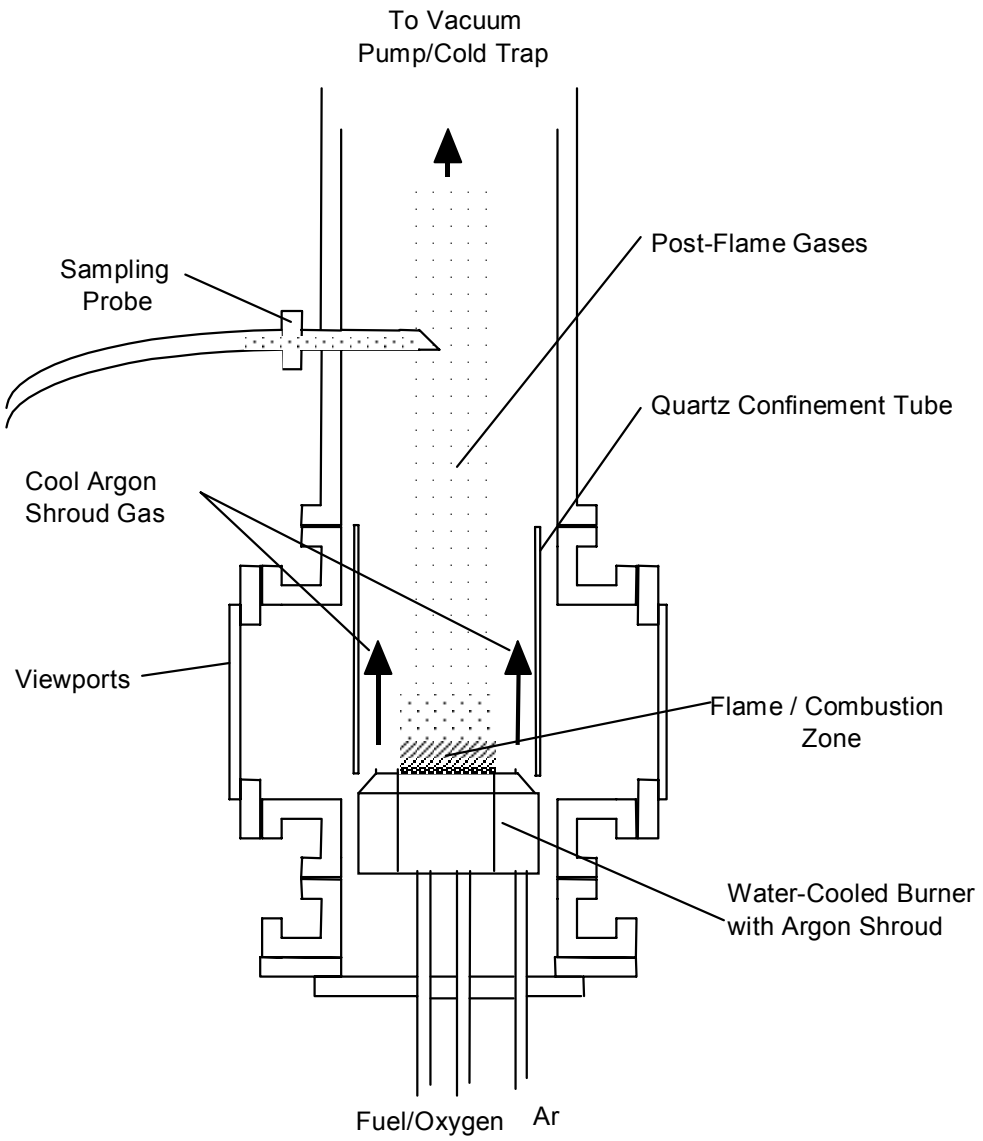

Figure 2. Diagram of the low-pressure flame apparatus. The sampling probe is located 36 cm downstream of the burner in the cool post-flame region of the chamber.

also prevents radicals from diffusing to the vacuum chamber walls, minimizing wall reactions. A quartz microprobe sample tube is located 36 cm downstream of the burner face with its inlet tip usually centered in the gas flow. A fine hole in the tip of the quartz microprobe is used to sample the cooled reaction gases. A 2-m length of room-temperature Teflon tubing, maintained at 8–20 Torr by pumping, conducts the gas sample from the flame chamber to the analytical instrumentation.

The radical-rich portion of the flame, where vigorous combustion occurs, is within 1–2 cm of the burner face, depending on the pressure. In this region of the flame, there is little mixing of core and shroud gas flows, and the core flow can be considered essentially one dimensional. The radical content of the flame drops rapidly beyond this region. In the region 3–5 cm downstream of the burner, substantial mixing of the shroud gas rapidly cools the combustion products, and wall reactions are minimized by the quartz liner. The quartz liner ends 15 cm downstream from the burner, where the combustion products are cooled enough to be essentially non-reactive with the stainless-steel walls of the vacuum chamber.

In preliminary experiments that examined radial diffusion of the core gases, we flowed nitrogen in the shroud and doped argon into a mixture of hydrogen and oxygen in the core flow. The sample probe was translated across the radial dimension of the flame while observing the relative argon signal with the mass spectrometer. Figure 3 illustrates the extent of the radial diffusion of the argon into the shroud nitrogen gas at flame pressures of 10 and 50 Torr. The radial diffusion of the core gas is logically more extensive at 10 Torr. At 50 Torr, the core gas flow remains relatively concentrated within the 3-cm radius of the burner core radial dimension, even at the distant downstream sampling location of 36 cm. In modeling the combustion, it would be reasonable to assume relatively little inter-diffusion of core and shroud gases in the hottest reaction regions a few cm downstream of the burner face; however, diffusion may impact temperature and species concentrations in the cooler downstream regions of the flame.

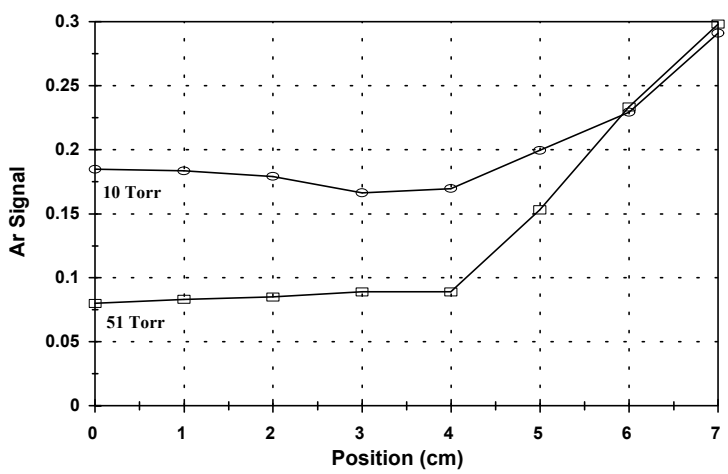

Figure 3. Argon signal vs radial position of sample tube. Center of vacuum chamber and burner are at 7 cm; outer edge of burner core is at 4 cm; wall of chamber is at 0 cm. Sampling tube is located 36 cm downstream of the burner face.

2.2 Results

The fuel flow to the core of the burner was set to 1.6 Standard Liters Per Minute (SLM) in all experiments. The fuel was either pure H_2, or a 1:1 mixture of H_2 and CO. The stoichiometry of the flame was varied by varying the oxygen flow to the burner core from 0.65 to 1.6 SLM. Nitrogen was added to the core oxygen+fuel flow at 2.0 SLM to look for NO_x production and was also turned off for brief periods to establish the background signal levels. The pressure was maintained at 50 Torr in all experiments by adjusting the pumping speed as flows were changed

Initial experiments attempted to detect NO_x using mass spectrometry. By adding known flows of 5% NO in argon to core gas mixtures of $H_2/O_2/N_2$ with no flame running, it was determined that the minimum concentrations of NO that could be detected by our mass spectrometer system were on the order of 25 PPM. The limiting interference was primarily $^{15}N_2$ from the N_2 added to the core gas mixture. Repeated attempts to positively detect NO generated in a flame were inconclusive with the mass spectrometer.

To detect NO_x with much higher sensitivity, we used a Thermo-Electron Model 10 NO_x chemiluminescence analyzer. The analyzer operates in two detection modes, measuring either NO or the sum of several nitrogen oxides grouped here as NO_x (i.e., NO, NO_2, HNO_2, and HNO_3). Since this unit was designed to operate at atmospheric pressure, it was necessary to modify the analyzer's input gas handling system. The internal chemiluminescence detector portion of the analyzer nominally operates at 4 to 20 Torr, which is a useful input pressure range for the flame experiment. Therefore, the built-in flow restrictors that normally interface to atmospheric pressure were bypassed, and the Teflon tube with the sample flow from the vacuum chamber was attached directly to the detector input manifold. A mechanical absolute vacuum gauge (Wallace & Tiernan Model FA160150) was used to monitor pressure in the sample transfer line. It was found that in NO detection mode the transfer line pressure was about 8 Torr, whereas in the NO_x detection mode, which requires interaction of the sample with a catalyst bed, the transfer line pressure was typically 28 Torr. The transfer line pressure affects the accuracy of the measurement because the detector signal yields the total NO, or NO_x, flow in the transfer line, which depends on the conditions present at the orifice located at the tip of the quartz microprobe. The flow through an orifice depends on temperature, differential pressure, and gas composition in a complex manner.[7] Most importantly, the mass flow in the tube is independent of the transfer line pressure *only* if the transfer line pressure is less than about half the pressure in the chamber. Although this was true in NO detection mode, it was not strictly true in NO_x detection mode. Experiments with known NO flows showed that the error was only 5–10% in NO_x detection mode. The temperature and gas composition also affect the mass flow through the orifice, and the effects of these variations on the NO_x flows were calculated from the measured experimental temperatures and gas compositions, and the data were corrected to reflect these changes.

The chemiluminescence analyzer was calibrated with a known NO mixture prior to use. The noise and sensitivity of the analyzer were close to the stated specifications of the instrument. It was possible to measure NO_x at concentrations less than a part-per-million (PPM) volume, although noise started to become significant below a few PPM. The noise (mainly short-term drift) and zero point of the analyzer were established by making measurements with N_2 absent from the core flame in between measurements with N_2 present. The mean zero point was subtracted from NO and NO_x measurements, and the zero point uncertainty is reflected in the error bars on the data. The error bars

are larger for NO_x measurements because it was difficult to reproducibly purge the instrument's catalytic cell, used in NO_x detection mode, in order to determine the NO_x zero point.

Figures 4 and 5 show the cool downstream flows of NO and NO_x for flames at 50 Torr pressure fueled with H_2 and with a 1:1 mixture of H_2+CO, respectively. The flame stoichiometry is given by the parameter

$$\lambda = \frac{[O_2]/[fuel]}{([O_2]/[fuel])_{stoichiometric}}.$$

A value of $\lambda = 1$ corresponds to stoichiometric combustion, where $([O_2]/[fuel])_{stoichiometric} = 0.5$ for either pure H_2 fuel, or any H_2/CO mixture. The NO curve in the figures shows the measured NO concentration. The NO_x curve shows the sum of NO, NO_2 HNO_2 and HNO_3. NO is seen to be the primary nitrogen oxide formed in the flame. Due to the width of the error bars on the NO_x plot, it is difficult to be sure whether significant NO_x other than NO is present.

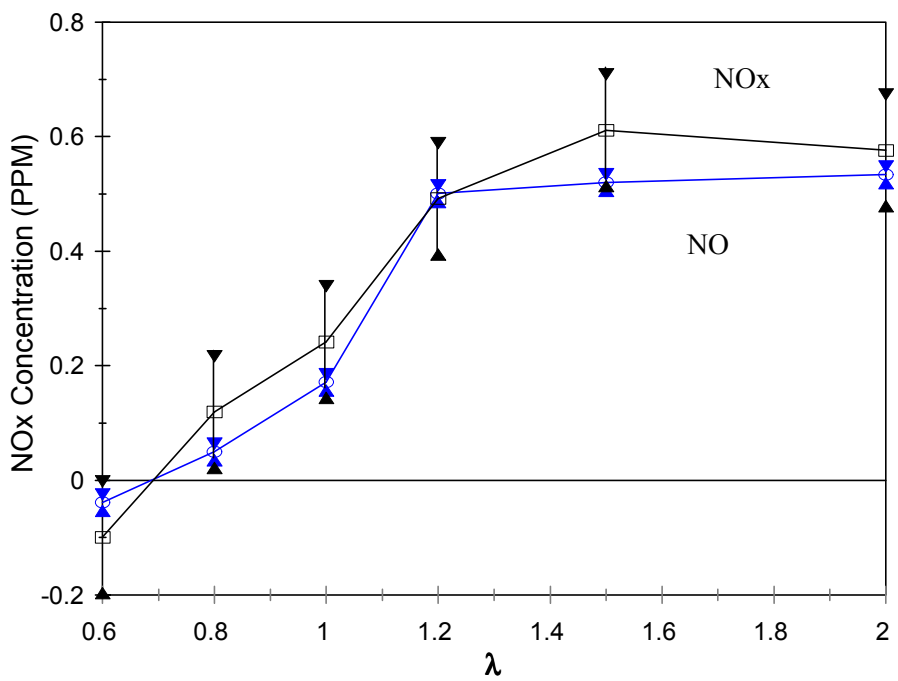

Figure 4. NO and NO_x yields as a function of flame stoichiometry for H_2-fueled flame. The measurements are indicated by square and circle symbols, and the uncertainty limits are indicated by triangles.

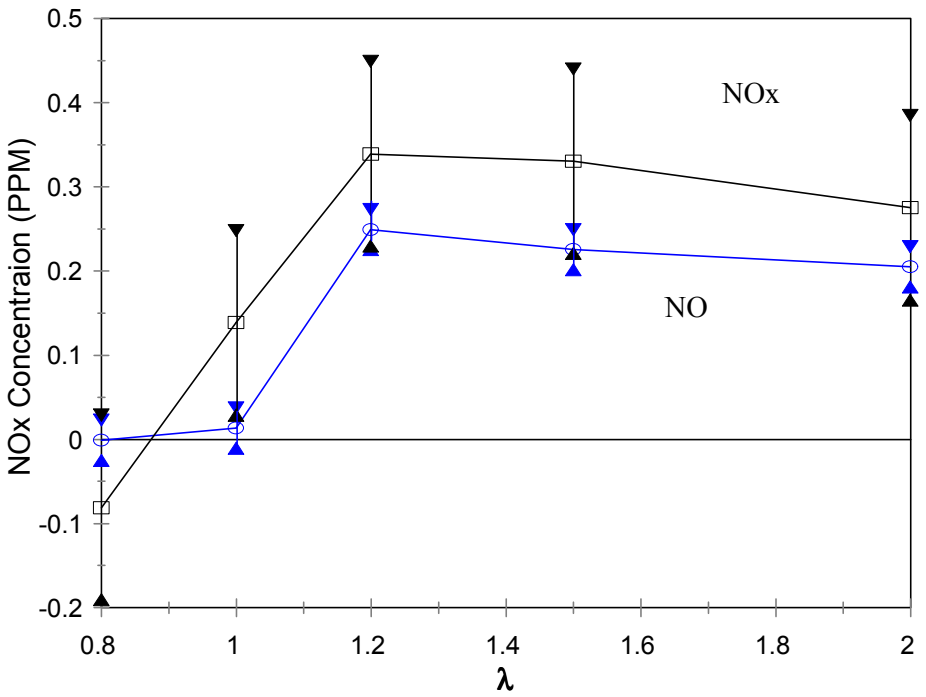

Figure 5. NO and NO_x yields as a function of flame stoichiometry for H_2+CO fueled flame. The measurements are indicated by square and circle symbols, and the uncertainty limits are indicated by triangles.

3. Flame Model

3.1 Description

To model the reaction chemistry in the laboratory flame, we used the Sandia Labs CHEMKIN[8,9] chemistry reaction solver, which has become a standard in the combustion research field. To model the flow, we used the Sandia PREMIX flow model, which simulates a one-dimensional, burner-stabilized laminar flame with premixed reactants and employs CHEMKIN to solve the chemical reaction equations.

Table 1 lists the flow conditions used as input to the PREMIX/CHEMKIN model at a total pressure of 50 Torr. The GRI-Mech 2.11 chemical reaction set[10] was used by CHEMKIN. The rate constant data are given in the Appendix. This reaction set includes 277 elementary reactions for CHNO combustion and is optimized for use with methane flames, but is extensive enough to be a good starting point for modeling nitrogen combustion in our $H_2/CO/O_2/N_2$ laboratory flame.

The PREMIX/CHEMKIN model can be run in two different modes: adiabatic mode and fixed-temperature mode. In the adiabatic mode, a chemistry solution is obtained with no heat lost from the gas system. Since PREMIX is a one-dimensional model (i.e., axial flow direction), it does not nominally include the effects of radial heat loss at the edge of the flame, or the effects of cool shroud gas entrained into the flame. In the alternate fixed-temperature mode, the axial temperature profile can be artificially constrained to an experimentally measured profile, and the chemistry is solved with this constraint. The fixed-temperature mode was used in our model calculations, employing axial temperature profiles measured with a sliding thermocouple.

3.2 Model Results

Model predictions of NO and NO_x concentrations 36 cm downstream of the burner face are plotted against the stoichiometry parameter λ in Figures 6 and 7. Figure 6 shows the results for hydrogen-fueled flames, and Figure 7 shows the results for flames fueled with a 1:1 mixture of hydrogen and carbon monoxide.

Table 1. Model Input Flows (SLM) [a]

λ	0.6	0.8	1.0	1.2	1.5	2.0
O_2	0.48	0.64	0.8	0.96	1.2	1.6
Fuel [b]	1.6	1.6	1.6	1.6	1.6	1.6
N_2	2.0	2.0	2.0	2.0	2.0	2.0

[a] Burner core area is 29.2 cm^2; flame pressure is 50 Torr.

[b] Fuel is either H_2 , or a 1:1 mixture of H_2 and CO.

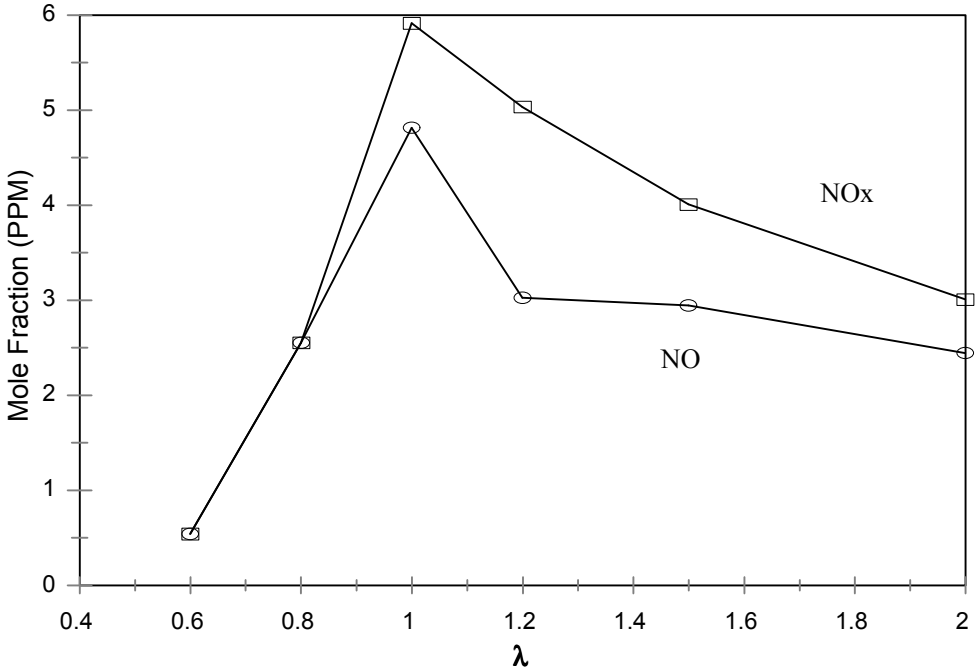

Figure 6. Modeled NO and NO_x yields for H_2-fueled flame.

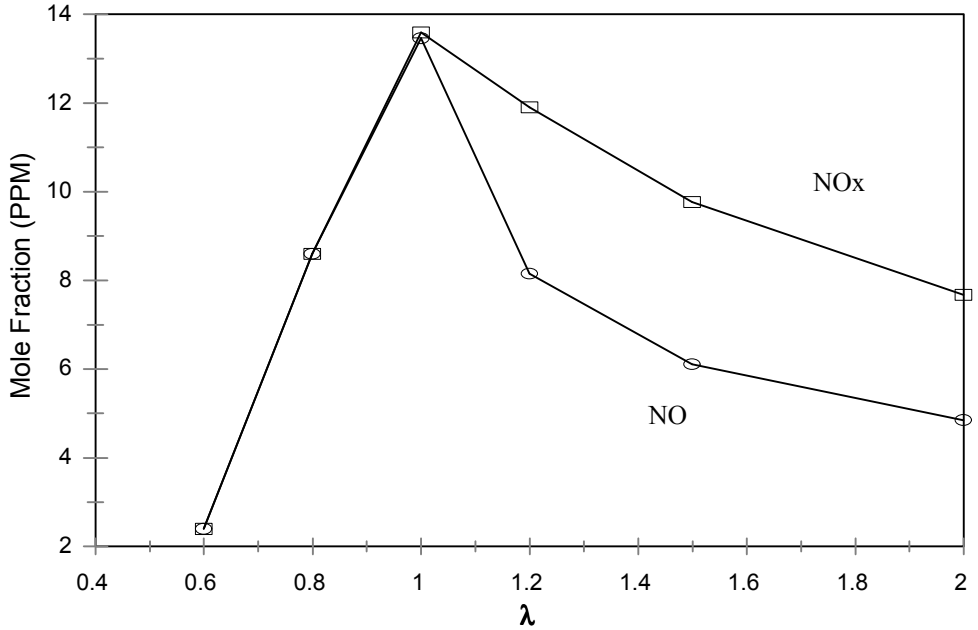

Figure 7. Modeled NO and NO_x yields for a 1:1 H_2+CO fueled flame.

4. Discussion

The experimentally measured NO and NO_x concentrations were close to the rated minimum detection limit of the analyzer and more than an order of magnitude below those predicted by the PREMIX/CHEMKIN model. It is unlikely that we failed to detect all available NO_x produced by the flame since detectable NO_x compounds formed in the flame (NO, NO_2, HNO_2, and HNO_3) are stable enough to survive transport through the quartz microprobe and Teflon transfer tube to the detector. Although quantitative agreement is poor, there is qualitative agreement between experiment and model prediction on several points. First, there is agreement on the trend of increasing NO_x production with increasing λ, the normalized oxygen-to-fuel ratio. Second, the model and experiments agree that NO is the dominant oxide of nitrogen formed in the flame. Third, there is agreement that approximately twice the amounts of NO and NO_x are formed when H_2 + CO is used as a fuel as when H_2 is used alone. Finally, although a peak in NO_x production predicted by PREMIX/CHEMKIN at $\lambda \approx 1.0$ was not clearly observed in the experimental data, there are hints of a peak in the hydrogen-fueled flame and a clear plateau with either fuel. The qualitative agreement suggests that the basic chemical model in CHEMKIN may be substantially complete, but that modifications may be required either in the reaction rate constants for the major NO_x production pathways, or in the simplistic flow model.

The GRI-Mech 2.11 chemical reaction set is considered by its authors to be a preliminary model for nitrogen combustion, even though it contains an extensive set of nitrogen reaction kinetics. The authors report substantially more difficulty in obtaining agreement between experiment and model results for nitrogen combustion than for C + H + O combustion alone. Most of the validations done by the authors of GRI-Mech 2.11 were performed in the hot, radical-rich portion of flames near a burner. In order to more completely address combustion throughout an afterburning rocket plume, our experiment examined the reaction products downstream of the flame in the cooler, slow combustion region. Accurate modeling of our experimental results requires that the reaction rate constants be accurately known over a very wide temperature range, which may not be true of all important nitrogen combustion reactions in GRI-Mech 2.11. GRI recently released a new version of its CHNO combustion model, which is more extensively validated. We will test the new reaction set in future model calculations.

Four principle chemical pathways to NO_x formation in C/H/N/O flames have been identified:[6] the Zeldovich high-temperature mechanism involving attack of O atoms on N_2 (Appendix; Reactions 176–178); the CH path, in which HCN and N are converted to NO (Appendix; Reaction 238); three-body recombination involving the formation of N_2O (Appendix; Reactions 180, 183, and 197); and the low-temperature N_2H mechanism[11] (Appendix; Reactions 202–209). The reaction rate constants for the simple Zeldovich mechanism are quite well known. The CH mechanism requires hydrocarbons, which are not present in the H_2 fueled flame and unlikely to be formed in any significant amount in the H_2+CO fueled flame. Therefore, the three-body recombination and N_2H mechanism rate constants are the most likely candidates for modification.

The second important issue in the use of PREMIX /CHEMKIN is the one-dimensional nature of the PREMIX flow model. The configuration of our flame experiment may not be adequately represented by the PREMIX code. PREMIX models a one-dimensional, laminar, premixed flame and, thus, does not take into account radial spreading of the flame, cooling by the walls of the vacuum chamber, or dilution and cooling of the flame by argon shroud gas mixing with the core oxygen+fuel flow. We attempted to compensate for the temperature differences induced by shroud gas mixing by forcing PREMIX to use an axial temperature profile derived from actual measurements in the flame. Although general trends are typically reproduced in this way, the technique of artificially constraining the temperature of the solution is not physically rigorous for obtaining a quantitative solution.

The dominant source of NO_X in the present one-dimensional model calculations is the NNH mechanism, which is initiated by the three-body recombination of N_2 and H to form NNH. It is likely that the modeled formation of NNH (and subsequently NO_X) would be reduced with a more accurate model of the two-dimensional flow in the flame. Formation of NNH would presumably be reduced as a consequence of dilution by entrained shroud gas in the cool downstream region of the flame where recombination is most important. The rate constants for the new and incompletely validated NNH mechanism may also require adjustment after the flow dynamics are accurately modeled.

A physically rigorous solution to the flow problem requires expanding the flame model to (at least) a two-dimensional solution with a computational fluid dynamic calculation. Several models are available for this computationally intensive problem. We have investigated the VULCAN three-dimensional combustor software and the PHOENICS generalized three-dimensional flow/combustion software. VULCAN is optimized for hypersonic combustion and is suitable for jet engine design, but may be amenable to rapid modeling of the laboratory flame with small reaction sets. PHOENICS is more suited to modeling the laboratory flame and also uses the CHEMKIN chemistry solver. We are presently adapting the PHOENICS CFD code with a reduced reaction set to model NO_x and SO_x formation in the laboratory flame.

5. Summary

Experiments were performed to measure the conversion of molecular nitrogen to NO_x in low-pressure, premixed $H_2 + O_2 + N_2$ and $H_2 + CO + O_2 + N_2$ flames, set up to simulate a stratospheric rocket plume afterburning environment. A chemiluminescence detection method was employed to detect NO_x production at sub-PPM levels as a function of oxygen:fuel ratio at a pressure of 50 Torr.

The measured yields of NO_x in the laboratory flame were compared to the yields of NO_x predicted by the PREMIX/CHEMKIN one-dimensional laminar flame simulation code from Sandia Labs. The simulation substantially over-predicted the measured formation of NO_x, although there was qualitative agreement on observed trends with oxygen:fuel ratio and fuel type. The PREMIX/CHEMKIN model used in the simulations is one dimensional and therefore does not model either radial diffusion of species and heat, or mixing of the shroud gas into the core flame. It is apparent that a more rigorous, two-dimensional simulation of the gas and heat flow in the flame is necessary. We have recently begun to use the PHOENICS multi-dimensional CFD code with the CHEMKIN chemistry solver to examine the combustion of nitrogen and sulfur in our flame.

The NO_x formation mechanisms (and related reaction rate constants) that are important in the low-pressure, H_2 and H_2+CO fueled laboratory flames are also expected to be the dominant NO_x mechanisms in the afterburning plumes of essentially all rocket motor types at stratospheric altitudes. Eventual validation of these mechanisms and rate constants will increase the accuracy of the rocket plume afteburning models that employ these fundamental parameters.

This page intentionally blank.

References

1. M. L. Burke and P. F. Zittel, *Combustion and Flame*, 112, 210-220 (1998).
2. P. M. Sheaffer and P. F. Zittel, "Combustion of Sulfur Compounds in a Low-Pressure Hydrogen-Oxygen Flame," TOR-2000(1490)-1, The Aerospace Corporation, El Segundo, CA, 15 January 2000.
3. P. M. Sheaffer and P. F. Zittel, "Combustion of SO_2 in a Low-Pressure Hydrogen-Oxygen Flame: Part II–Computer Modeling," TOR-2000(1490)-2, The Aerospace Corporation, El Segundo, CA, 10 November 2000.
4. P. F. Zittel, "Computer Model Calculations of NO_x Production in Rocket Motors and Plumes," TOR-96(1306)-1, The Aerospace Corporation, El Segundo, CA, 30 November 1995.
5. W. C. Gardiner, Jr., *Combustion Chemistry*, Springer-Verlag, NY, 1984.
6. R. Fristrom, Flame *Structure and Processes*, Oxford University Press, 1995.
7. J. F. O'Hanlon, *A User's Guide to Vacuum Technology*, 2nd Ed, John Wiley & Sons, 1989.
8. R. J. Kee, F. M. Rupley, and J. A. Miller, SANDIA Report SAND89-8009B, 1989.
9. R. J. Kee, et. al., SANDIA Report SAND85-8240, 1994.
10. C.T. Bowman, R.K. Hanson, D.F. Davidson, W.C. Gardiner, Jr., V. Lissianski, G.P. Smith, D.M. Golden, M. Frenklach and M. Goldenberg, http://www.me.berkeley.edu/gri_mech/.
11. J. E. Harrington, G. P. Smith, P. A. Berg, A. R. Noble, J. B. Jeffries, and D. R. Crosley, "Evidence for a New NO Production Mechanism in Flames," Twenty-sixth Symposium (International) on Combustion, 1996, pg. 2133.

This page intentionally blank.

Appendix

Reaction Rate Constants Used in CHEMKIN/PREMIX Model

$(k = A\ T^{m}\ e^{-E/RT})$

	Reaction	A (cgs units)	m	E (cal/mole)
1	2O+M<=>O2+M	1.200E+17	-1.000	0.00
2	O+H+M<=>OH+M	5.000E+17	-1.000	0.00
3	O+H2<=>H+OH	5.000E+04	2.670	6290.00
4	O+HO2<=>OH+O2	2.000E+13	0.000	0.00
5	O+H2O2<=>OH+HO2	9.630E+06	2.000	4000.00
6	O+CH<=>H+CO	5.700E+13	0.000	0.00
7	O+CH2<=>H+HCO	8.000E+13	0.000	0.00
8	O+CH2(S)<=>H2+CO	1.500E+13	0.000	0.00
9	O+CH2(S)<=>H+HCO	1.500E+13	0.000	0.00
10	O+CH3<=>H+CH2O	8.430E+13	0.000	0.00
11	O+CH4<=>OH+CH3	1.020E+09	1.500	8600.00
12	O+CO+M<=>CO2+M	6.020E+14	0.000	3000.00
13	O+HCO<=>OH+CO	3.000E+13	0.000	0.00
14	O+HCO<=>H+CO2	3.000E+13	0.000	0.00
15	O+CH2O<=>OH+HCO	3.900E+13	0.000	3540.00
16	O+CH2OH<=>OH+CH2O	1.000E+13	0.000	0.00
17	O+CH3O<=>OH+CH2O	1.000E+13	0.000	0.00
18	O+CH3OH<=>OH+CH2OH	3.880E+05	2.500	3100.00
19	O+CH3OH<=>OH+CH3O	1.300E+05	2.500	5000.00
20	O+C2H<=>CH+CO	5.000E+13	0.000	0.00
21	O+C2H2<=>H+HCCO	1.020E+07	2.000	1900.00
22	O+C2H2<=>OH+C2H	4.600E+19	-1.410	28950.00
23	O+C2H2<=>CO+CH2	1.020E+07	2.000	1900.00
24	O+C2H3<=>H+CH2CO	3.000E+13	0.000	0.00
25	O+C2H4<=>CH3+HCO	1.920E+07	1.830	220.00
26	O+C2H5<=>CH3+CH2O	1.320E+14	0.000	0.00
27	O+C2H6<=>OH+C2H5	8.980E+07	1.920	5690.00
28	O+HCCO<=>H+2CO	1.000E+14	0.000	0.00
29	O+CH2CO<=>OH+HCCO	1.000E+13	0.000	8000.00
30	O+CH2CO<=>CH2+CO2	1.750E+12	0.000	1350.00
31	O2+CO<=>O+CO2	2.500E+12	0.000	47800.00
32	O2+CH2O<=>HO2+HCO	1.000E+14	0.000	40000.00
33	H+O2+M<=>HO2+M	2.800E+18	-0.860	0.00
34	H+2O2<=>HO2+O2	3.000E+20	-1.720	0.00

	Reaction	A (cgs units)	m	E (cal/mole)
35	H+O2+H2O<=>HO2+H2O	9.380E+18	-0.760	0.00
36	H+O2+N2<=>HO2+N2	3.750E+20	-1.720	0.00
37	H+O2+AR<=>HO2+AR	7.000E+17	-0.800	0.00
38	H+O2<=>O+OH	8.300E+13	0.000	14413.00
39	2H+M<=>H2+M	1.000E+18	-1.000	0.00
40	2H+H2<=>2H2	9.000E+16	-0.600	0.00
41	2H+H2O<=>H2+H2O	6.000E+19	-1.250	0.00
42	2H+CO2<=>H2+CO2	5.500E+20	-2.000	0.00
43	H+OH+M<=>H2O+M	2.200E+22	-2.000	0.00
44	H+HO2<=>O+H2O	3.970E+12	0.000	671.00
45	H+HO2<=>O2+H2	2.800E+13	0.000	1068.00
46	H+HO2<=>2OH	1.340E+14	0.000	635.00
47	H+H2O2<=>HO2+H2	1.210E+07	2.000	5200.00
48	H+H2O2<=>OH+H2O	1.000E+13	0.000	3600.00
49	H+CH<=>C+H2	1.100E+14	0.000	0.00
50	H+CH2(+M)<=>CH3(+M)	2.500E+16	-0.800	0.00
51	H+CH2(S)<=>CH+H2	3.000E+13	0.000	0.00
52	H+CH3(+M)<=>CH4(+M)	1.270E+16	-0.630	383.00
53	H+CH4<=>CH3+H2	6.600E+08	1.620	10840.00
54	H+HCO(+M)<=>CH2O(+M)	1.090E+12	0.480	-260.00
55	H+HCO<=>H2+CO	7.340E+13	0.000	0.00
56	H+CH2O(+M)<=>CH2OH(+M)	5.400E+11	0.454	3600.00
57	H+CH2O(+M)<=>CH3O(+M)	5.400E+11	0.454	2600.00
58	H+CH2O<=>HCO+H2	2.300E+10	1.050	3275.00
59	H+CH2OH(+M)<=>CH3OH(+M)	1.800E+13	0.000	0.00
60	H+CH2OH<=>H2+CH2O	2.000E+13	0.000	0.00
61	H+CH2OH<=>OH+CH3	1.200E+13	0.000	0.00
62	H+CH2OH<=>CH2(S)+H2O	6.000E+12	0.000	0.00
63	H+CH3O(+M)<=>CH3OH(+M)	5.000E+13	0.000	0.00
64	H+CH3O<=>H+CH2OH	3.400E+06	1.600	0.00
65	H+CH3O<=>H2+CH2O	2.000E+13	0.000	0.00
66	H+CH3O<=>OH+CH3	3.200E+13	0.000	0.00
67	H+CH3O<=>CH2(S)+H2O	1.600E+13	0.000	0.00
68	H+CH3OH<=>CH2OH+H2	1.700E+07	2.100	4870.00
69	H+CH3OH<=>CH3O+H2	4.200E+06	2.100	4870.00
70	H+C2H(+M)<=>C2H2(+M)	1.000E+17	-1.000	0.00
71	H+C2H2(+M)<=>C2H3(+M)	5.600E+12	0.000	2400.00
72	H+C2H3(+M)<=>C2H4(+M)	6.080E+12	0.270	280.00
73	H+C2H3<=>H2+C2H2	3.000E+13	0.000	0.00
74	H+C2H4(+M)<=>C2H5(+M)	1.080E+12	0.454	1820.00
75	H+C2H4<=>C2H3+H2	1.325E+06	2.530	12240.00
76	H+C2H5(+M)<=>C2H6(+M)	5.210E+17	-0.990	1580.00
77	H+C2H5<=>H2+C2H4	2.000E+12	0.000	0.00
78	H+C2H6<=>C2H5+H2	1.150E+08	1.900	7530.00
79	H+HCCO<=>CH2(S)+CO	1.000E+14	0.000	0.00
80	H+CH2CO<=>HCCO+H2	5.000E+13	0.000	8000.00
81	H+CH2CO<=>CH3+CO	1.130E+13	0.000	3428.00

	Reaction	A (cgs units)	m	E (cal/mole)
82	H+HCCOH<=>H+CH2CO	1.000E+13	0.000	0.00
83	H2+CO(+M)<=>CH2O(+M)	4.300E+07	1.500	79600.00
84	OH+H2<=>H+H2O	2.160E+08	1.510	3430.00
85	2OH(+M)<=>H2O2(+M)	7.400E+13	-0.370	0.00
86	2OH<=>O+H2O	3.570E+04	2.400	-2110.00
87	OH+HO2<=>O2+H2O	2.900E+13	0.000	-500.00
88	OH+H2O2<=>HO2+H2O	1.750E+12	0.000	320.00
89	OH+C<=>H+CO	5.000E+13	0.000	0.00
90	OH+CH<=>H+HCO	3.000E+13	0.000	0.00
91	OH+CH2<=>H+CH2O	2.000E+13	0.000	0.00
92	OH+CH2<=>CH+H2O	1.130E+07	2.000	3000.00
93	OH+CH2(S)<=>H+CH2O	3.000E+13	0.000	0.00
94	OH+CH3(+M)<=>CH3OH(+M)	6.300E+13	0.000	0.00
95	OH+CH3<=>CH2+H2O	5.600E+07	1.600	5420.00
96	OH+CH3<=>CH2(S)+H2O	2.501E+13	0.000	0.00
97	OH+CH4<=>CH3+H2O	1.000E+08	1.600	3120.00
98	OH+CO<=>H+CO2	4.760E+07	1.228	70.00
99	OH+HCO<=>H2O+CO	5.000E+13	0.000	0.00
100	OH+CH2O<=>HCO+H2O	3.430E+09	1.180	-447.00
101	OH+CH2OH<=>H2O+CH2O	5.000E+12	0.000	0.00
102	OH+CH3O<=>H2O+CH2O	5.000E+12	0.000	0.00
103	OH+CH3OH<=>CH2OH+H2O	1.440E+06	2.000	-840.00
104	OH+CH3OH<=>CH3O+H2O	6.300E+06	2.000	1500.00
105	OH+C2H<=>H+HCCO	2.000E+13	0.000	0.00
106	OH+C2H2<=>H+CH2CO	2.180E-04	4.500	-1000.00
107	OH+C2H2<=>H+HCCOH	5.040E+05	2.300	13500.00
108	OH+C2H2<=>C2H+H2O	3.370E+07	2.000	14000.00
109	OH+C2H2<=>CH3+CO	4.830E-04	4.000	-2000.00
110	OH+C2H3<=>H2O+C2H2	5.000E+12	0.000	0.00
111	OH+C2H4<=>C2H3+H2O	3.600E+06	2.000	2500.00
112	OH+C2H6<=>C2H5+H2O	3.540E+06	2.120	870.00
113	OH+CH2CO<=>HCCO+H2O	7.500E+12	0.000	2000.00
114	2HO2<=>O2+H2O2	1.300E+11	0.000	-1630.00
115	HO2+CH2<=>OH+CH2O	2.000E+13	0.000	0.00
116	HO2+CH3<=>O2+CH4	1.000E+12	0.000	0.00
117	HO2+CH3<=>OH+CH3O	2.000E+13	0.000	0.00
118	HO2+CO<=>OH+CO2	1.500E+14	0.000	23600.00
119	HO2+CH2O<=>HCO+H2O2	1.000E+12	0.000	8000.00
120	C+O2<=>O+CO	5.800E+13	0.000	576.00
121	C+CH2<=>H+C2H	5.000E+13	0.000	0.00
122	C+CH3<=>H+C2H2	5.000E+13	0.000	0.00
123	CH+O2<=>O+HCO	3.300E+13	0.000	0.00
124	CH+H2<=>H+CH2	1.107E+08	1.790	1670.00
125	CH+H2O<=>H+CH2O	1.713E+13	0.000	-755.00
126	CH+CH2<=>H+C2H2	4.000E+13	0.000	0.00
127	CH+CH3<=>H+C2H3	3.000E+13	0.000	0.00
128	CH+CH4<=>H+C2H4	6.000E+13	0.000	0.00

	Reaction	A (cgs units)	m	E (cal/mole)
129	CH+CO(+M)<=>HCCO(+M)	5.000E+13	0.000	0.00
130	CH+CO2<=>HCO+CO	3.400E+12	0.000	690.00
131	CH+CH2O<=>H+CH2CO	9.460E+13	0.000	-515.00
132	CH+HCCO<=>CO+C2H2	5.000E+13	0.000	0.00
133	CH2+O2<=>OH+HCO	1.320E+13	0.000	1500.00
134	CH2+H2<=>H+CH3	5.000E+05	2.000	7230.00
135	2CH2<=>H2+C2H2	3.200E+13	0.000	0.00
136	CH2+CH3<=>H+C2H4	4.000E+13	0.000	0.00
137	CH2+CH4<=>2CH3	2.460E+06	2.000	8270.00
138	CH2+CO(+M)<=>CH2CO(+M)	8.100E+11	0.500	4510.00
139	CH2+HCCO<=>C2H3+CO	3.000E+13	0.000	0.00
140	CH2(S)+N2<=>CH2+N2	1.500E+13	0.000	600.00
141	CH2(S)+AR<=>CH2+AR	9.000E+12	0.000	600.00
142	CH2(S)+O2<=>H+OH+CO	2.800E+13	0.000	0.00
143	CH2(S)+O2<=>CO+H2O	1.200E+13	0.000	0.00
144	CH2(S)+H2<=>CH3+H	7.000E+13	0.000	0.00
145	CH2(S)+H2O(+M)<=>CH3OH(+M)	2.000E+13	0.000	0.00
146	CH2(S)+H2O<=>CH2+H2O	3.000E+13	0.000	0.00
147	CH2(S)+CH3<=>H+C2H4	1.200E+13	0.000	-570.00
148	CH2(S)+CH4<=>2CH3	1.600E+13	0.000	-570.00
149	CH2(S)+CO<=>CH2+CO	9.000E+12	0.000	0.00
150	CH2(S)+CO2<=>CH2+CO2	7.000E+12	0.000	0.00
151	CH2(S)+CO2<=>CO+CH2O	1.400E+13	0.000	0.00
152	CH2(S)+C2H6<=>CH3+C2H5	4.000E+13	0.000	-550.00
153	CH3+O2<=>O+CH3O	2.675E+13	0.000	28800.00
154	CH3+O2<=>OH+CH2O	3.600E+10	0.000	8940.00
155	CH3+H2O2<=>HO2+CH4	2.450E+04	2.470	5180.00
156	2CH3(+M)<=>C2H6(+M)	2.120E+16	-0.970	620.00
157	2CH3<=>H+C2H5	4.990E+12	0.100	10600.00
158	CH3+HCO<=>CH4+CO	2.648E+13	0.000	0.00
159	CH3+CH2O<=>HCO+CH4	3.320E+03	2.810	5860.00
160	CH3+CH3OH<=>CH2OH+CH4	3.000E+07	1.500	9940.00
161	CH3+CH3OH<=>CH3O+CH4	1.000E+07	1.500	9940.00
162	CH3+C2H4<=>C2H3+CH4	2.270E+05	2.000	9200.00
163	CH3+C2H6<=>C2H5+CH4	6.140E+06	1.740	10450.00
164	HCO+H2O<=>H+CO+H2O	2.244E+18	-1.000	17000.00
165	HCO+M<=>H+CO+M	1.870E+17	-1.000	17000.00
166	HCO+O2<=>HO2+CO	7.600E+12	0.000	400.00
167	CH2OH+O2<=>HO2+CH2O	1.800E+13	0.000	900.00
168	CH3O+O2<=>HO2+CH2O	4.280E-13	7.600	-3530.00
169	C2H+O2<=>HCO+CO	5.000E+13	0.000	1500.00
170	C2H+H2<=>H+C2H2	4.070E+05	2.400	200.00
171	C2H3+O2<=>HCO+CH2O	3.980E+12	0.000	-240.00
172	C2H4(+M)<=>H2+C2H2(+M)	8.000E+12	0.440	88770.00
173	C2H5+O2<=>HO2+C2H4	8.400E+11	0.000	3875.00
174	HCCO+O2<=>OH+2CO	1.600E+12	0.000	854.00
175	2HCCO<=>2CO+C2H2	1.000E+13	0.000	0.00

	Reaction	A (cgs units)	m	E (cal/mole)
176	N+NO<=>N2+O	3.500E+13	0.000	330.00
177	N+O2<=>NO+O	2.650E+12	0.000	6400.00
178	N+OH<=>NO+H	7.333E+13	0.000	1120.00
179	N2O+O<=>N2+O2	1.400E+12	0.000	10810.00
180	N2O+O<=>2NO	2.900E+13	0.000	23150.00
181	N2O+H<=>N2+OH	4.400E+14	0.000	18880.00
182	N2O+OH<=>N2+HO2	2.000E+12	0.000	21060.00
183	N2O(+M)<=>N2+O(+M)	1.300E+11	0.000	59620.00
184	HO2+NO<=>NO2+OH	2.110E+12	0.000	-480.00
185	NO+O+M<=>NO2+M	1.060E+20	-1.410	0.00
186	NO2+O<=>NO+O2	3.900E+12	0.000	-240.00
187	NO2+H<=>NO+OH	1.320E+14	0.000	360.00
188	NH+O<=>NO+H	5.000E+13	0.000	0.00
189	NH+H<=>N+H2	3.200E+13	0.000	330.00
190	NH+OH<=>HNO+H	2.000E+13	0.000	0.00
191	NH+OH<=>N+H2O	2.000E+09	1.200	0.00
192	NH+O2<=>HNO+O	4.610E+05	2.000	6500.00
193	NH+O2<=>NO+OH	1.280E+06	1.500	100.00
194	NH+N<=>N2+H	1.500E+13	0.000	0.00
195	NH+H2O<=>HNO+H2	2.000E+13	0.000	13850.00
196	NH+NO<=>N2+OH	2.160E+13	-0.230	0.00
197	NH+NO<=>N2O+H	4.160E+14	-0.450	0.00
198	NH2+O<=>OH+NH	7.000E+12	0.000	0.00
199	NH2+O<=>H+HNO	4.600E+13	0.000	0.00
200	NH2+H<=>NH+H2	4.000E+13	0.000	3650.00
201	NH2+OH<=>NH+H2O	9.000E+07	1.500	-460.00
202	NNH<=>N2+H	3.300E+08	0.000	0.00
203	NNH+M<=>N2+H+M	1.300E+14	-0.110	4980.00
204	NNH+O2<=>HO2+N2	5.000E+12	0.000	0.00
205	NNH+O<=>OH+N2	2.500E+13	0.000	0.00
206	NNH+O<=>NH+NO	7.000E+13	0.000	0.00
207	NNH+H<=>H2+N2	5.000E+13	0.000	0.00
208	NNH+OH<=>H2O+N2	2.000E+13	0.000	0.00
209	NNH+CH3<=>CH4+N2	2.500E+13	0.000	0.00
210	H+NO+M<=>HNO+M	8.950E+19	-1.320	740.00
211	HNO+O<=>NO+OH	2.500E+13	0.000	0.00
212	HNO+H<=>H2+NO	4.500E+11	0.720	660.00
213	HNO+OH<=>NO+H2O	1.300E+07	1.900	-950.00
214	HNO+O2<=>HO2+NO	1.000E+13	0.000	13000.00
215	CN+O<=>CO+N	7.700E+13	0.000	0.00
216	CN+OH<=>NCO+H	4.000E+13	0.000	0.00
217	CN+H2O<=>HCN+OH	8.000E+12	0.000	7460.00
218	CN+O2<=>NCO+O	6.140E+12	0.000	-440.00
219	CN+H2<=>HCN+H	2.100E+13	0.000	4710.00
220	NCO+O<=>NO+CO	2.350E+13	0.000	0.00
221	NCO+H<=>NH+CO	5.400E+13	0.000	0.00
222	NCO+OH<=>NO+H+CO	2.500E+12	0.000	0.00

	Reaction	A (cgs units)	m	E (cal/mole)
223	NCO+N<=>N2+CO	2.000E+13	0.000	0.00
224	NCO+O2<=>NO+CO2	2.000E+12	0.000	20000.00
225	NCO+M<=>N+CO+M	8.800E+16	-0.500	48000.00
226	NCO+NO<=>N2O+CO	2.850E+17	-1.520	740.00
227	NCO+NO<=>N2+CO2	5.700E+18	-2.000	800.00
228	HCN+M<=>H+CN+M	1.040E+29	-3.300	126600.00
229	HCN+O<=>NCO+H	1.107E+04	2.640	4980.00
230	HCN+O<=>NH+CO	2.767E+03	2.640	4980.00
231	HCN+O<=>CN+OH	2.134E+09	1.580	26600.00
232	HCN+OH<=>HOCN+H	1.100E+06	2.030	13370.00
233	HCN+OH<=>HNCO+H	4.400E+03	2.260	6400.00
234	HCN+OH<=>NH2+CO	1.600E+02	2.560	9000.00
235	H+HCN+M<=>H2CN+M	1.400E+26	-3.400	1900.00
236	H2CN+N<=>N2+CH2	6.000E+13	0.000	400.00
237	C+N2<=>CN+N	6.300E+13	0.000	46020.00
238	CH+N2<=>HCN+N	2.857E+08	1.100	20400.00
239	CH+N2(+M)<=>HCNN(+M)	3.100E+12	0.150	0.00
240	CH2+N2<=>HCN+NH	1.000E+13	0.000	74000.00
241	CH2(S)+N2<=>NH+HCN	1.000E+11	0.000	65000.00
242	C+NO<=>CN+O	1.900E+13	0.000	0.00
243	C+NO<=>CO+N	2.900E+13	0.000	0.00
244	CH+NO<=>HCN+O	5.000E+13	0.000	0.00
245	CH+NO<=>H+NCO	2.000E+13	0.000	0.00
246	CH+NO<=>N+HCO	3.000E+13	0.000	0.00
247	CH2+NO<=>H+HNCO	3.100E+17	-1.380	1270.00
248	CH2+NO<=>OH+HCN	2.900E+14	-0.690	760.00
249	CH2+NO<=>H+HCNO	3.800E+13	-0.360	580.00
250	CH2(S)+NO<=>H+HNCO	3.100E+17	-1.380	1270.00
251	CH2(S)+NO<=>OH+HCN	2.900E+14	-0.690	760.00
252	CH2(S)+NO<=>H+HCNO	3.800E+13	-0.360	580.00
253	CH3+NO<=>HCN+H2O	9.600E+13	0.000	28800.00
254	CH3+NO<=>H2CN+OH	1.000E+12	0.000	21750.00
255	HCNN+O<=>CO+H+N2	2.200E+13	0.000	0.00
256	HCNN+O<=>HCN+NO	2.000E+12	0.000	0.00
257	HCNN+O2<=>O+HCO+N2	1.200E+13	0.000	0.00
258	HCNN+OH<=>H+HCO+N2	1.200E+13	0.000	0.00
259	HCNN+H<=>CH2+N2	1.000E+14	0.000	0.00
260	HNCO+O<=>NH+CO2	9.800E+07	1.410	8500.00
261	HNCO+O<=>HNO+CO	1.500E+08	1.570	44000.00
262	HNCO+O<=>NCO+OH	2.200E+06	2.110	11400.00
263	HNCO+H<=>NH2+CO	2.250E+07	1.700	3800.00
264	HNCO+H<=>H2+NCO	1.050E+05	2.500	13300.00
265	HNCO+OH<=>NCO+H2O	4.650E+12	0.000	6850.00
266	HNCO+OH<=>NH2+CO2	1.550E+12	0.000	6850.00
267	HNCO+M<=>NH+CO+M	1.180E+16	0.000	84720.00
268	HCNO+H<=>H+HNCO	2.100E+15	-0.690	2850.00
269	HCNO+H<=>OH+HCN	2.700E+11	0.180	2120.00

	Reaction	A (cgs units)	m	E (cal/mole)
270	HCNO+H<=>NH2+CO	1.700E+14	-0.750	2890.00
271	HOCN+H<=>H+HNCO	2.000E+07	2.000	2000.00
272	HCCO+NO<=>HCNO+CO	2.350E+13	0.000	0.00
273	CH3+N<=>H2CN+H	6.100E+14	-0.310	290.00
274	CH3+N<=>HCN+H2	3.700E+12	0.150	-90.00
275	NH3+H<=>NH2+H2	5.400E+05	2.400	9915.00
276	NH3+OH<=>NH2+H2O	5.000E+07	1.600	955.00
277	NH3+O<=>NH2+OH	9.400E+06	1.940	6460.00

LABORATORY OPERATIONS

The Aerospace Corporation functions as an "architect-engineer" for national security programs, specializing in advanced military space systems. The Corporation's Laboratory Operations supports the effective and timely development and operation of national security systems through scientific research and the application of advanced technology. Vital to the success of the Corporation is the technical staff's wide-ranging expertise and its ability to stay abreast of new technological developments and program support issues associated with rapidly evolving space systems. Contributing capabilities are provided by these individual organizations:

Electronics and Photonics Laboratory: Microelectronics, VLSI reliability, failure analysis, solid-state device physics, compound semiconductors, radiation effects, infrared and CCD detector devices, data storage and display technologies; lasers and electro-optics, solid state laser design, micro-optics, optical communications, and fiber optic sensors; atomic frequency standards, applied laser spectroscopy, laser chemistry, atmospheric propagation and beam control, LIDAR/LADAR remote sensing; solar cell and array testing and evaluation, battery electrochemistry, battery testing and evaluation.

Space Materials Laboratory: Evaluation and characterizations of new materials and processing techniques: metals, alloys, ceramics, polymers, thin films, and composites; development of advanced deposition processes; nondestructive evaluation, component failure analysis and reliability; structural mechanics, fracture mechanics, and stress corrosion; analysis and evaluation of materials at cryogenic and elevated temperatures; launch vehicle fluid mechanics, heat transfer and flight dynamics; aerothermodynamics; chemical and electric propulsion; environmental chemistry; combustion processes; space environment effects on materials, hardening and vulnerability assessment; contamination, thermal and structural control; lubrication and surface phenomena.

Space Science Applications Laboratory: Magnetospheric, auroral and cosmic ray physics, wave-particle interactions, magnetospheric plasma waves; atmospheric and ionospheric physics, density and composition of the upper atmosphere, remote sensing using atmospheric radiation; solar physics, infrared astronomy, infrared signature analysis; infrared surveillance, imaging, remote sensing, and hyperspectral imaging; effects of solar activity, magnetic storms and nuclear explosions on the Earth's atmosphere, ionosphere and magnetosphere; effects of electromagnetic and particulate radiations on space systems; space instrumentation, design fabrication and test; environmental chemistry, trace detection; atmospheric chemical reactions, atmospheric optics, light scattering, state-specific chemical reactions and radiative signatures of missile plumes.

Center for Microtechnology: Microelectromechanical systems (MEMS) for space applications; assessment of microtechnology space applications; laser micromachining; laser-surface physical and chemical interactions; micropropulsion; micro- and nanosatellite mission analysis; intelligent microinstruments for monitoring space and launch system environments.

Office of Spectral Applications: Multispectral and hyperspectral sensor development; data analysis and algorithm development; applications of multispectral and hyperspectral imagery to defense, civil space, commercial, and environmental missions.